Available online at www.sciencedirect.com
ScienceDirect
Journal of the European Ceramic Society 29 (2009) 131–138
www.elsevier.com/locate/jeurceramsoc

Synthesis and characterisation of $BaCeO_3$-based proton conductors obtained from freeze-dried precursors

M. Amsif[a], D. Marrero-López[a], A. Magrasó[a,b], J. Peña-Martínez[a], J.C. Ruiz-Morales[a], P. Núñez[a,*]

[a] *Departamento de Química Inorgánica, Universidad de La Laguna, 38200-La Laguna, Tenerife, Spain*
[b] *FERMiO, Department of Chemistry, University of Oslo, Gaustadalleen 21, NO-0349 Oslo, Norway*

Received 23 March 2008; received in revised form 3 June 2008; accepted 9 June 2008
Available online 24 July 2008

Abstract

A freeze-drying precursor method was used to obtain submicrometric powders of $BaCeO_3$ and $BaCe_{0.9}Y_{0.1}O_{3-\delta}$ proton conductors at temperatures as low as 800 °C. The phase formation and evolution with the temperature was studied by X-ray diffraction (XRD) and thermal analysis (TG-DTA). The microstructure of both powders and sintered pellets was examined by scanning electron microscopy (SEM). Dense ceramic materials were obtained at 1400 °C and the different contributions to the overall conductivity, bulk and grain boundary, were studied using impedance spectroscopy under different atmospheres.

Keywords: Proton conductor; $BaCeO_3$; Precursor synthesis; Impedance spectroscopy

1. Introduction

Materials that present proton conductivity under H_2 and/or H_2O atmospheres have been widely studied as potential electrolyte materials for fuel cells, hydrogen sensors, electrochemical hydrogen pumps, electrochemical micro-reactors, etc.[1–7].

Compounds based on cerates, with perovskite-type structure, are among the state-of-the art proton conducting materials studied during the last few years.[8] The conduction properties of acceptor-doped $BaCeO_3$ have been widely investigated as they exhibit the highest proton conductivity reported so far.[9] Oxygen vacancies are introduced into this perovskite structure by aliovalent doping, i.e. partial replacement of cerium by: Y^{3+}, Yb^{3+}, Gd^{3+}, Nd^{3+}, etc.[10]. The solid solutions for $BaCe_{1-x}M_xO_{3-\delta}$ typically cover the range $0 \leq x \leq 0.2$.[11,12] The proton conduction in alkaline earth cerates occurs either via the hydration of oxygen vacancies after the material is exposed to water containing atmospheres (Eq. (1)), and/or by reduction of oxide ions in the lattice (Eq. (2)), according to the following equations:

$$H_2O(g) + v_O^{\bullet\bullet} + O_O^x = 2OH_O^{\bullet} \quad (1)$$

$$H_2(g) + 2O_O^x = 2OH_O^{\bullet} + 2e' \quad (2)$$

In addition, rare-earth-doped $BaCeO_3$ exhibit mixed ionic–electronic conductivity, depending on temperature and environmental conditions.[13,14] Proton conductivity is predominant at low temperature and oxide ion conductivity is the main contribution at high temperature.[15] A significant p-type electronic conductivity is also observed under oxidising conditions. The formation of electron holes at high oxygen partial pressure can be described by the following reaction:

$$\tfrac{1}{2}O_2(g) + v_O^{\bullet\bullet} = O_O^x + 2h^{\bullet} \quad (3)$$

The n-type conductivity is also relatively high under very reducing conditions.[1] Consequently, the occurrence of electronic conductivity places restrictions on the application of cerates as electrolyte materials at high temperature and low and high oxygen partial pressures. The material is operating well at temperatures below 800 °C.

The synthesis of $BaCeO_3$-based materials have been reported by several wet chemical methods, such as citric acid,[16,17] Pechini[18] and oxalate precursors,[19] but the dominating synthesis

* Corresponding author. Fax: +34 922 31 8461.
E-mail address: pnunez@ull.es (P. Núñez).

0955-2219/$ – see front matter © 2008 Elsevier Ltd. All rights reserved.
doi:10.1016/j.jeurceramsoc.2008.06.001

route used is the solid-state ceramic method,[13,20,21] which requires higher firing temperatures to obtain both a pure phase and high densification. This method has additional disadvantages, such as formation of undesirable phases, poor chemical homogeneity and large grain ceramic sizes. In the case of $BaCeO_3$-based materials, it has also been found that BaO evaporates at sintering temperature higher than 1550 °C,[22] so that reducing the sintering temperature is particularly important.

It is well known that the preparative route plays a critical role in the materials properties, controlling the structure, morphology and grain size of the obtained materials. The transport properties of ceramic materials also depend on ceramic microstructure, specially the grain boundary contribution. Hence, alternative synthesis routes can improve both the microstructure and conductivity of these materials. In this context, the use of precursors obtained by freeze-drying processing of the appropriate aqueous metal salts has proved to be a very versatile method for obtaining stoichiometrically controlled complex polymetallic systems.[23,24]

Here, yttrium was chosen as dopant in $BaCeO_3$, since it was reported that dopants with smaller ionic radii in $BaCeO_3$ made protonic conduction more favourable by lowering the oxide ionic conductivity.[25] Submicrometric powders of undoped and Y-doped $BaCeO_3$ have been prepared from a freeze-dried precursor route. The phase formation, densification, microstructure and conductivity under different atmospheres of the sintered bodies have been studied in the present report.

2. Experimental

2.1. Synthesis

Polycrystalline powders of $BaCe_{1-x}Y_xO_{3-\delta}$ ($x = 0$ and 0.1) were prepared by a freeze-dried precursor route, using as reagents: $Ba(NO_3)_2$ (+99% Aldrich), $Ce(NO_3)_3{\cdot}6H_2O$ (99.99% Aldrich) and Y_2O_3 (99.99% Aldrich). Metal nitrates were previously studied by thermogravimetric analysis to determine the correct cation content. Stoichiometric quantities of Y_2O_3 were dissolved in diluted nitric acid, whereas $Ba(NO_3)_2$ and $Ce(NO_3)_3{\cdot}6H_2O$ were dissolved in distilled water. Ethylenediaminetetraacetic acid (EDTA) (99.7% Aldrich) was added to the resulting solutions in a 1:1 molar ratio ligand:metal as complex agent. The pH was then adjusted between 7 and 8 by adding ammonia solution. A typical solution of 100 ml has a cation concentration of 15 mmol of Ba^{2+} giving rise to approximately 5 g of oxide. Droplets of this solution were subsequently flash frozen in liquid nitrogen, retaining the cation homogeneity of the original solution, and then freeze-dried in a HetoLyolab freeze-dryer for 3 days. In this way amorphous precursor powders were obtained, which were immediately calcined at 300 °C to prevent rehydration.

An alternative approach to freeze-drying was used to remove the water, just for comparison of the preparative method. The starting solution was slowly heated at 70 °C with continuous stirring overnight to remove the water and promote polymerization. In this way a dried and transparent gel was obtained without any visible formation of precipitation. Then the gel was calcined at 300 °C to produce the pyrolysis of the organic matter. Note that a similar procedure was used by Liu et al.[26] in the synthesis of $SrCeO_3$-based ceramics.

The dried precursor powders obtained by both methods were calcined between 300 and 1100 °C, for 1 h, in order to study the phase formation and its evolution with the temperature. All the thermal treatments were carried out in alumina crucibles to prevent reaction of barium with platinum crucibles.

2.2. Powder characterisation

Room temperature X-ray diffraction patterns (XRD) were collected with a Philips X'Pert Pro automated diffractometer, equipped with a primary monochromator Cu $K\alpha_1$ radiation and an X'Celerator detector. The scans were performed in the 2θ range (15–100°) with 0.016° step for 2 h. Structure refinements were performed using the FullProf[27] and WinPlotr suite softwares.[28] The amorphous precursor powders were studied by simultaneous Thermogravimetric Analysis (TGA) and Differential Thermal Analysis (DTA) on a PerkinElmer instrument (mod. Pyris Diamond) at a heating rate of 10 °C/min in air. The morphology of both powders and sintered pellets was observed using a Scanning Electron Microscope (Jeol Ltd., JSM-6300) operating at an accelerating voltage of 20 kV. All preparations were covered with a thin film of gold to avoid charging problems and to obtain better image definition.

2.3. Electrical measurements

The polycrystalline oxide powders, calcined at 1100 °C for 1 h, were pressed into 10 mm diameter and 1.5 mm thick pellets at 250 MPa. The resulting pellets were sintered in air between 1300 and 1600 °C for 4 h. Pt-ink (Metalor) were painted on each side of the pellet and then fired at 800 °C for 30 min to ensure maximum conductivity and adherence. It should be commented that some reactivity was found between the Pt-electrodes and the ceramic electrolyte when they fired at 1000 °C, resulting in a new process in the impedance spectra with a capacitance value similar to that of the grain boundary. This contribution seems to be ascribed to a superficial layer between the ceramic electrolyte and the metal electrode due their chemical interaction. The impedance spectra were performed on a 1260 Solartron Impedance Analyser between 200 and 800 °C in the 0.1–10^6 Hz frequency range. Impedance data were acquired with ZPlot and analysed with ZView softwares.[29] Equivalent circuits consisting in serial (RQ) elements were used to fit the spectra and to study separately the different contributions, where R is a resistance and Q is a pseudocapacitance with impedance value of $Z_Q = 1/[Q(iw)^n]$. This is related to the real capacitance C as follows:

$$C = Q^{1/n}(R)^{(1-n)/n} \quad (4)$$

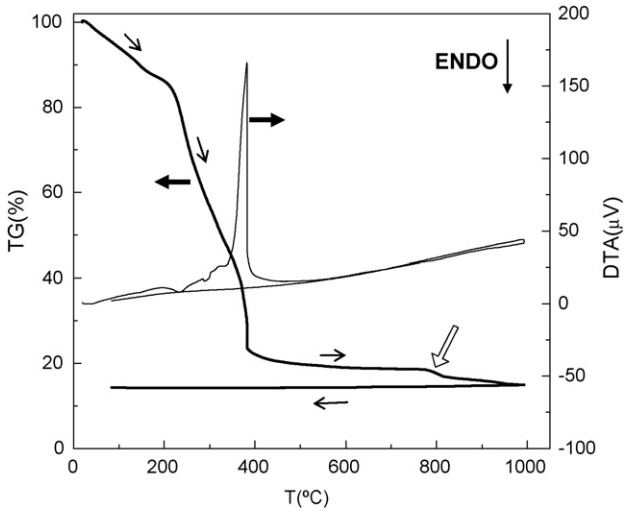

Fig. 1. TG/DTA curves of $BaCe_{0.9}Y_{0.1}O_{3-\delta}$ precursor powder obtained at a heating rate of 10 °C/min.

3. Results and discussion

3.1. Phase formation and structure

The TGA curves in air of the amorphous freeze-dried precursor powders present several weight loss steps (Fig. 1). A first steady weight loss occurs from room temperature to 200 °C. This is usually associated to the elimination of residual water, dehydration of the precursor and removal of NO_x species. A sharp fall in the specimen weight is observed over the temperature range 200–400 °C related to the oxidative decomposition of the organic material, which is an exothermic process in the DTA curve. A third decomposition step is detected around 800 °C attributed to the oxidation of $BaCO_3$, which remains in the precursor mixture up to 800 °C as observed by XRD analysis (Fig. 2). The precursor obtained by polymerization exhibits a decomposition temperature slightly higher than freeze-drying 850–900 °C, similar to that previously reported for the synthesis of $SrCeO_3$ from a similar procedure.[26]

The thermal evolution of XRD patterns for $BaCe_{0.9}Y_{0.1}O_{3-\delta}$ precursor obtained by freeze-drying and calcined between 300 and 1100 °C for 1 h are presented in Fig. 2a. After combustion at 300 °C the ceramic powders consist in a mixture of amorphous and crystalline precursors. Two different polycrystalline phases are detectable, CeO_2 fluorite-type and $Ba(NO_3)_2$. After calcination at 600 °C and removal of major part of carbon species, barium nitrate decomposed and then barium carbonate is formed under air atmosphere. The formation of $BaCeO_3$ perovskite-type structure occurs simultaneously or immediately after the decomposition of $BaCO_3$. As aforementioned, this agrees with the TGA results, where a small weight loss is observed around 800 °C. The freeze-drying method makes possible to synthesize the perovskite-type structure after one single thermal treatment at relatively low temperature. The perovskite phase is already formed at 800 °C, although there is still a minimal $BaCO_3$ precipitation detectable by means of high resolution XRD. This impurity disappears after calcination at 800 °C for several hours and/or 900–1000 °C for 1 h. On the contrary, the phases prepared by polymerization (Fig. 2b) exhibit a large quantity of $SrCO_3$ at 800 °C compared to freeze-drying method. A calcination temperature up to 1100 °C is required to obtain a nearly single phase. It should be noted that the synthesis temperature of $BaCeO_3$ from freeze-drying precursor is lower compared the conventional solid-state reaction method ~1400 °C[20,11] and even somewhat lower than other precursor routes previously reported in the literature. For instance, the synthesis temperatures reported for $BaCeO_3$ are: 1050 °C by mixed oxalate precursors,[19] 900 °C by an aqueous citrate–nitrate process[30] and

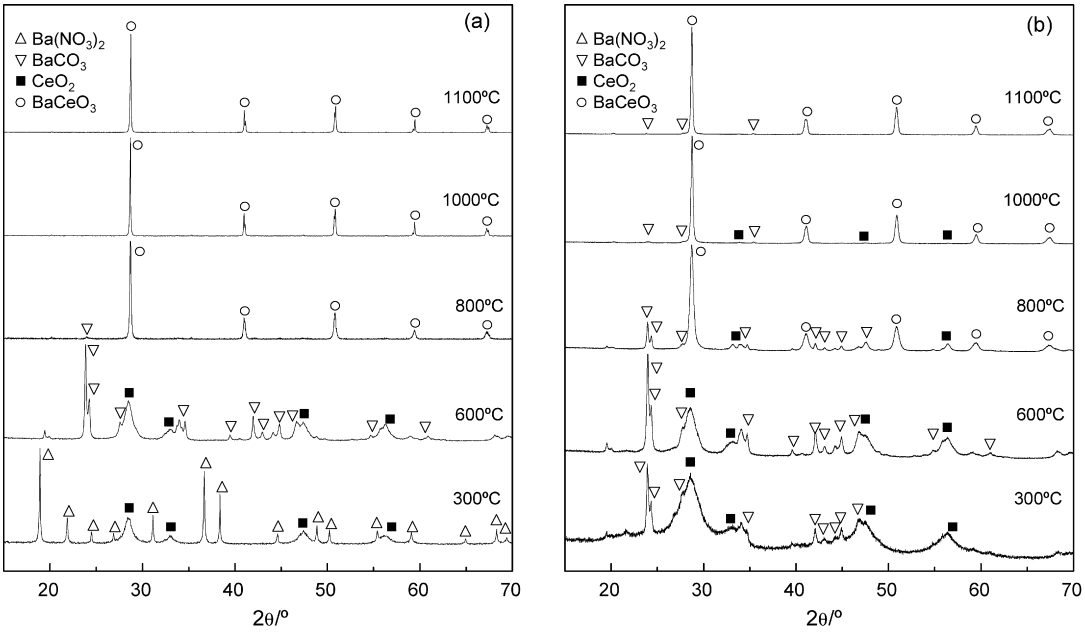

Fig. 2. Evolution of XRD patterns of $BaCe_{0.9}Y_{0.1}O_{3-\delta}$ prepared from (a) freeze-dried precursor and (b) polymerization route calcined at different temperatures between 300 and 1100 °C for1 h.

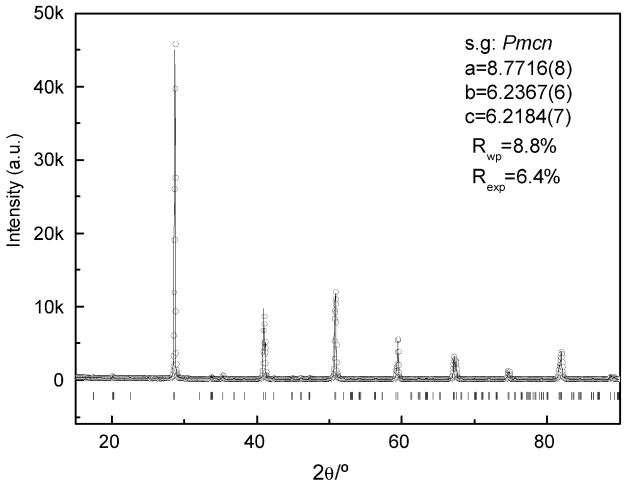

Fig. 3. Rietveld refinement of polycrystalline $BaCe_{0.9}Y_{0.1}O_{3-\delta}$ calcined at 1100 °C. The cell parameters and R-factors are listed in the inset.

950 °C by a water-soluble complex precursor.[26] It should be also commented that freeze-drying is a process which is suitable to dehydrate a wide variety of industrial products. These include agrochemicals, pharmaceutical intermediates, biological products, foods and flavourings; hence the preparation of large quantities of precursor for the synthesis of almost any ceramic material is possible.

The Rietveld refinements for $BaCe_{0.9}Y_{0.1}O_{3-\delta}$ calcined at 1100 °C was carried out using the structural models proposed in the literature (ICSD 72768) in the orthorhombic *Pmcn* space group. The usual parameters were refined: scale factors, background coefficients, zero-points, half-width, pseudo-Voigt, asymmetry parameters for the peak-shape and atomic positions. The Rietveld result is shown in Fig. 3 and the lattice cell parameters and R-factors are listed in the inset of Fig. 3 and they are in agreement with those reported previously in the ICSD database.

The polycrystalline powders calcined at 1100 °C were pressed into disks and sintered between 1300 and 1600 °C for 4 h to study the phase stability at high temperature. Then, they were finely ground and studied by XRD (Fig. 4). The corresponding XRD patterns do not show appreciable structural changes and any secondary phases up to 1500 °C. However, a small fraction of CeO_2 is observed at 1600 °C. This might be ascribed to evaporation of BaO at this temperature, as other authors observed experimentally for undoped barium cerate.[31] Hence, low synthesis temperature in the preparation of $BaCeO_3$-based ceramics is recommendable to avoid phase segregations, which can affect the transport properties. One should take into account that CeO_2 exhibits high electronic conductivity under reducing conditions.

3.2. Microstructural characterisation

The morphology of $BaCe_{0.9}Y_{0.1}O_{3-\delta}$ powders resulting from the freeze-drying synthesis route after calcined at 1100 °C for 1 h and without any previous mechanical treatment (e.g. ball-milling) are shown in Fig. 5. They consist in well-separated particles in the submicrometric range with an average diameter below 0.25 μm. Although a nearly single phase is obtained

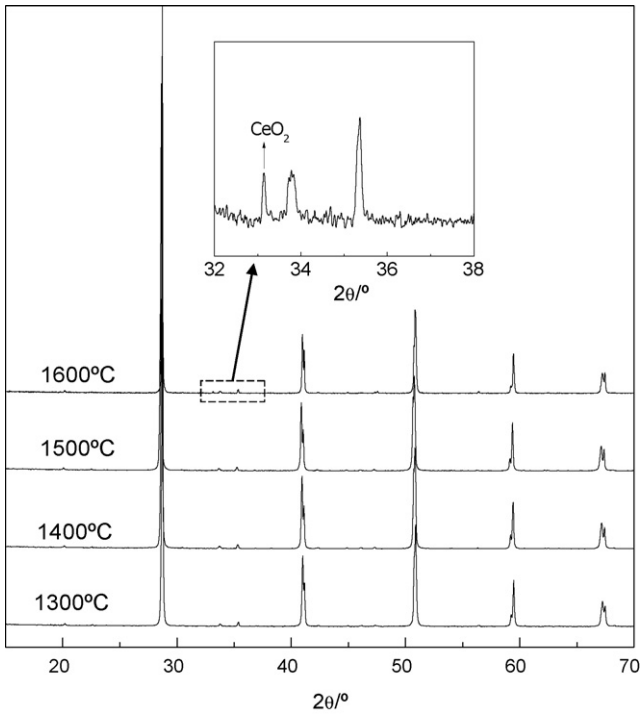

Fig. 4. XRD patterns of sintered pellets obtained between 1300 and 1600 °C for 4 h. A small fraction of CeO_2 is observed at 1600 °C.

at only 800 °C, the better densification of the ceramic pellet was obtained after calcination of the powders at 1100 °C for 1 h. This is due to a better morphology of the ceramic particles, which allows obtaining higher compaction density of the green pellets, improving densification at lower sintering temperatures.

The SEM images shown in Fig. 6 correspond to pellets of undoped and Y-doped $BaCeO_3$ at different sintered temperatures. No phase segregation at the grain boundaries was found in any of the samples investigated. The relative densities of the

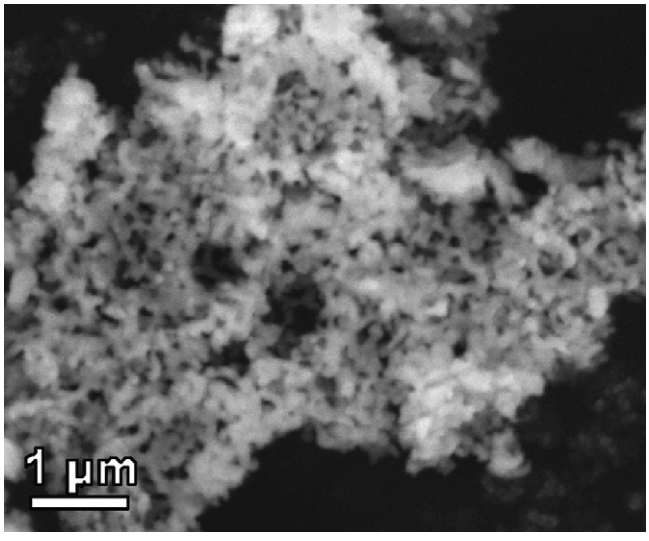

Fig. 5. SEM image of the microstructure of $BaCe_{0.9}Y_{0.1}O_{3-\delta}$ polycrystalline powders prepared by freeze-drying method and calcined at 1100 °C for 1 h.

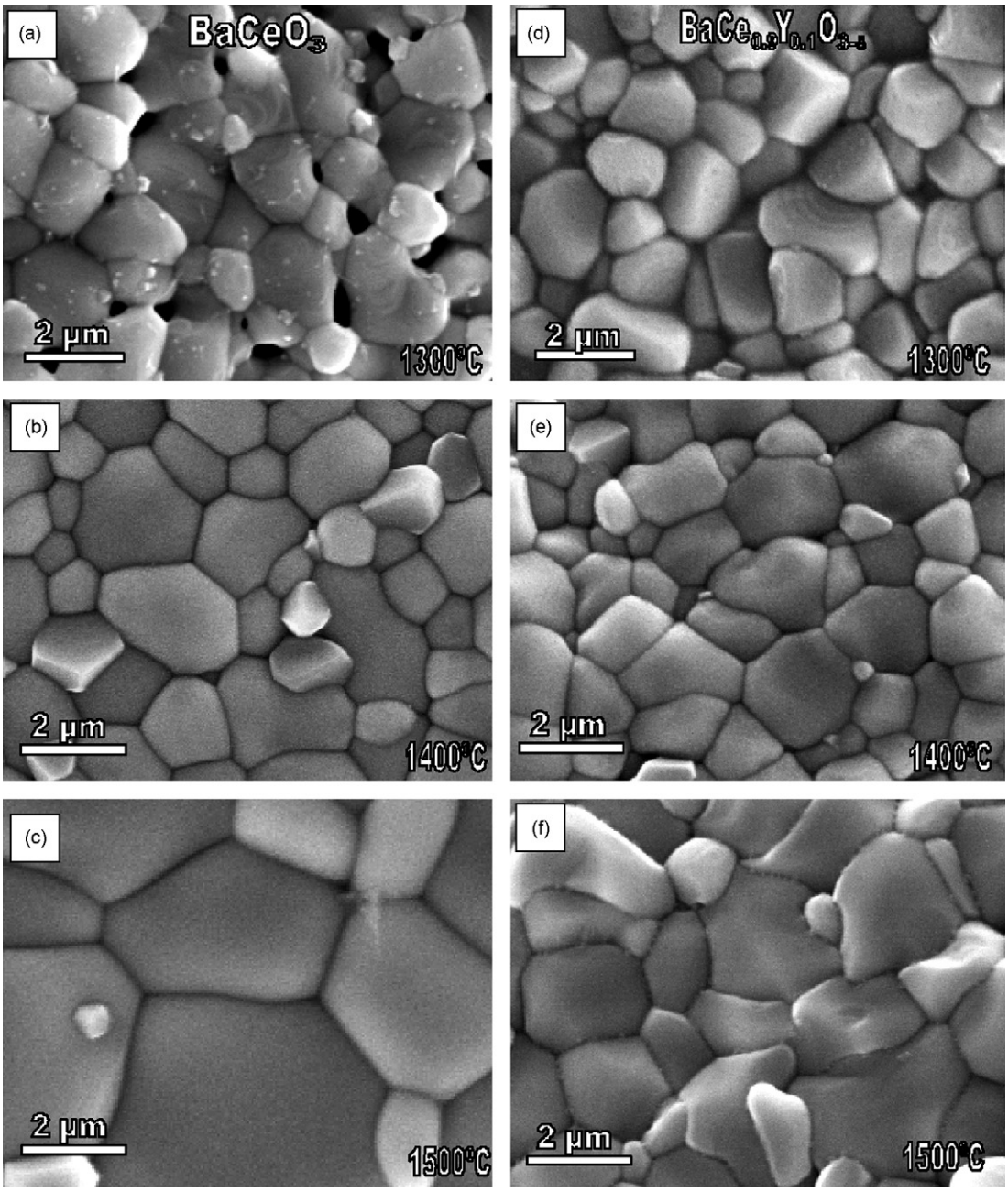

Fig. 6. SEM images of surface pellets of (a–c) $BaCeO_3$ and (d–f) $BaCe_{0.9}Y_{0.1}O_{3-\delta}$ sintered at 1300, 1400 and 1500 °C for 4 h.

sintered pellets are about 85% at 1300 °C, 98% at 1400 °C and 99% at 1500 °C. The ceramic microstructure is not significantly influenced by the Y-doping and sintering temperature. The main differences are found in the grain size, where Y-doping retards the grain growth, especially observable at very high sintering temperature (1500 °C) (Fig. 6f). This is generally associated to an enrichment of the trivalent dopant at grain boundary region, according to the space charge model.[32] The excess of dopant located at the grain boundary generates a concentration gradient between the grain interior and grain boundaries that retains the mobility of cations along the grain boundary, causing decreased grain growth rates. A similar effect has previously been observed in other materials, such as doped-CeO_2.[33] The average grain size increases with the sintering temperature from 1.5 μm at 1300 °C, 2 μm at 1400 °C and 2.5 μm at 1500 °C for $BaCe_{0.9}Y_{0.1}O_{3-\delta}$. Undoped $BaCeO_3$ samples exhibit larger grain sizes about 5 μm at 1500 °C (Fig. 6c).

Powders obtained by polymerization method have a low sinterability compared to freeze-drying powders and the relative density of the pellets was lower than 75% after sintered at 1400 °C for 4 h. This effect seems to be associated to powder agglomerates, which difficult the preparation of dense ceramic materials.[29] A ball-milling process might reduce the particles agglomeration, improving possibly the densification. Only samples prepared by freeze-drying were electrically characterised due to their better densification.

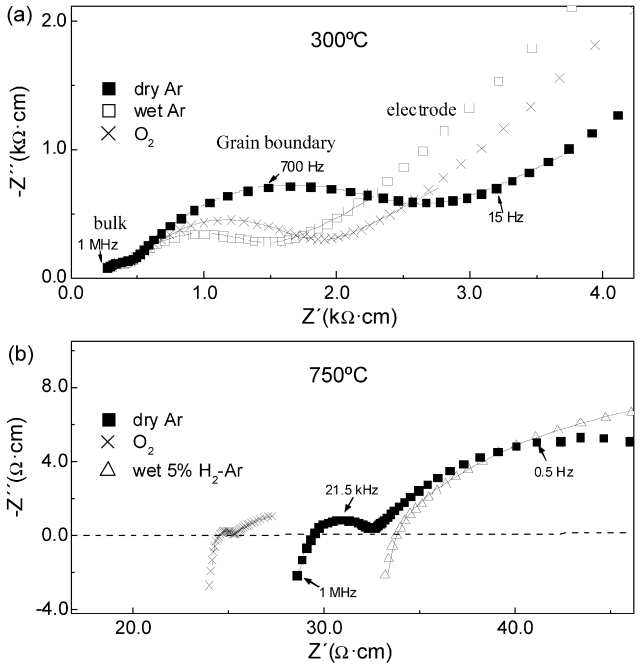

Fig. 7. Impedance spectra of $BaCe_{0.9}Y_{0.1}O_{3-\delta}$ sintered pellet at 1400 °C and measured at (a) 300 °C and (b) 750 °C under different atmospheres. The solid line is the fitting results obtained with equivalent circuits.

3.3. Electrical characterization

The impedance spectra in the low temperature range for $BaCe_{0.9}Y_{0.1}O_{3-\delta}$ sintered at 1400 °C (Fig. 7a) show three separated contributions ascribed to the grain interior at high frequency, grain boundary and electrode interface processes at low frequency. These impedance spectra were analysed using an equivalent circuit to obtain the resistance and capacitance of the different processes. The equivalent circuit used can be expressed as a serial combination of RQ elements in the form: $(R_bQ_b)(R_{gb}Q_{gb})(Q_e)$, where the subscripts b, gb and e denote bulk, grain boundary and material/electrode processes, respectively. The values of capacitance are about 5 pF cm^{-1}, 15 nF cm^{-1} and 1 μF cm^{-1} for the grain interior, grain boundary and electrode processes, respectively. As can be observed, the grain boundary is the main resistive contribution of the electrolyte in the low temperature range, and it varies significantly with atmosphere conditions. The grain boundary resistance is lower in hydrogen containing atmosphere than under argon. On the contrary, the bulk is less influenced by the atmosphere at low temperature. The high temperature impedance spectra present two contributions attributed to the electrode responses (Fig. 7b). Grain boundary and grain interior processes cannot be separated at high temperature, although generally the grain boundary contribution is lower compared to bulk at high temperature. In this case, the equivalent circuit used to fit the spectra is denoted as: $LR_s(R_{e1}Q_{e1})(R_{e2}Q_{e2})$, where L is an autoinductance element, which is associated to the autoinductive effects introduced, by the equipment, and R_s is a serial resistance equal to overall electrolyte resistance. Note that R_s takes approximately the same value as the Z'-intercept of the impedance spectra at high frequency. The contributions with relaxation frequencies of 45 kHz and 0.6 Hz are associated to electrode responses with capacitance values of 0.6 μF cm^{-1} and 7.4 mF cm^{-1} respectively.

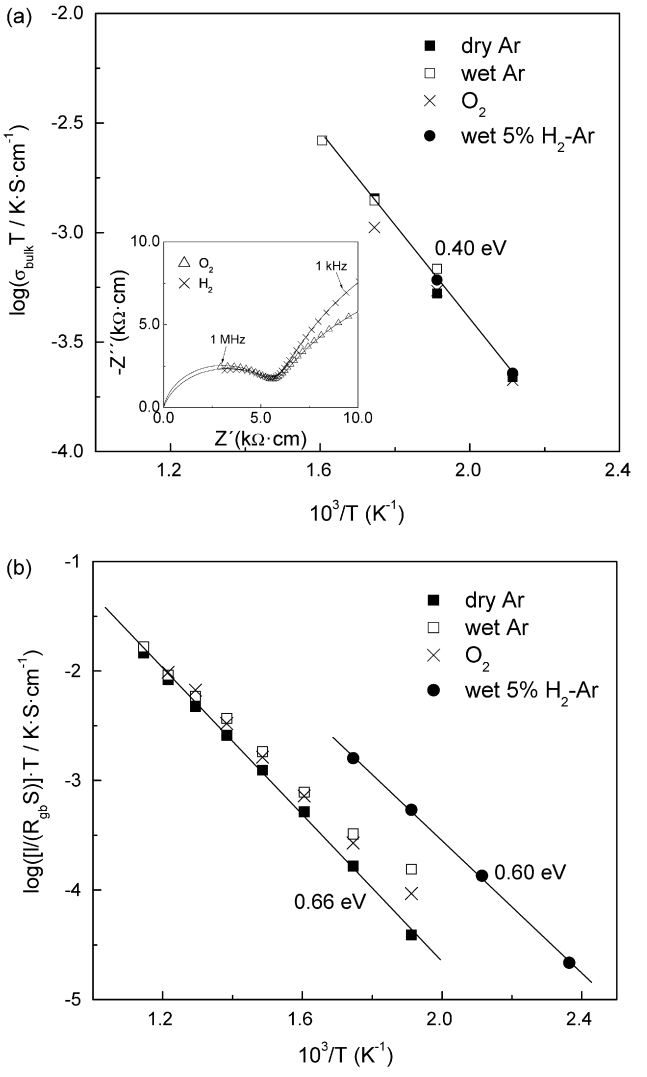

Fig. 8. Arrhenius plots of bulk conductivity (a) and the corresponding grain boundary results l/($R_{gb}S$) (b) under different atmospheres for $BaCe_{0.9}Y_{0.1}O_{3-\delta}$ sintered at 1400 °C for 4 h. The inset shows the impedance spectra of the bulk contribution in O_2 and wet 5%H_2–Ar.

The grain interior (R_b) and grain boundary (R_{gb}) resistances were used to obtain the bulk and macroscopic grain boundary conductivity, taking into account the sample geometry:

$$\sigma_i = \frac{l}{R_i S} \tag{5}$$

where l is the sample thickness and S is the electrode area. The values of conductivity were plotted using the Arrhenius equation:

$$\sigma = \frac{\sigma_0}{T} \cdot \exp\left(\frac{-E_a}{kT}\right) \tag{6}$$

The thermal dependence of grain interior conductivity is shown in Fig. 8a. As can be observed, the bulk conductivity is nearly independent on the atmosphere, at least in the low temperature range, where bulk and grain boundary can be

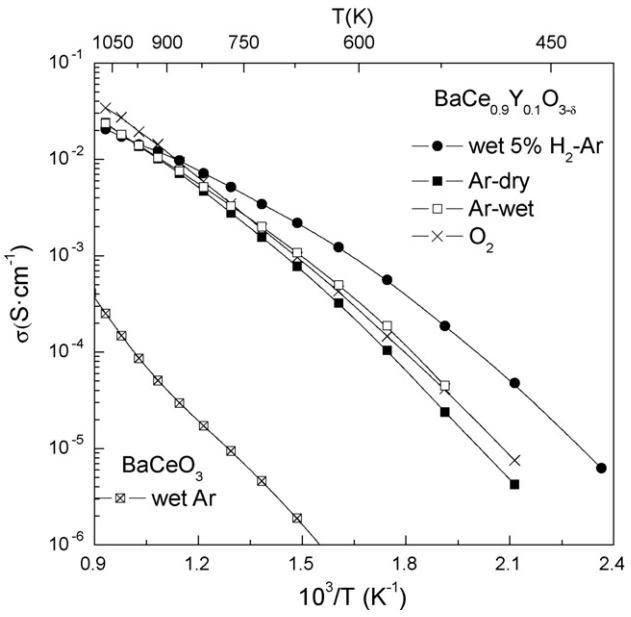

Fig. 9. Arrhenius representation of the overall conductivity for $BaCe_{0.9}Y_{0.1}O_{3-\delta}$ sintered pellet at 1400 °C under different atmospheres.

studied separately (inset Fig. 8a). The values of activation energies are also similar, and about 0.40 eV. On the contrary, the grain boundary resistance has a greater dependence on the environmental conditions, showing higher resistance values under dry Ar (1 ppm H_2O) and lower resistance in wet 5% H_2 (2% H_2O). The activation energy for the grain boundary conductivity (∼0.6 eV) is somewhat higher than that of the bulk contribution. These results seem to indicate that the transport properties of Y-doped barium cerates are very influenced by the grain boundary contribution at low temperature, where the grain boundary resistance is the main contribution to the overall conductivity.

The Arrhenius plots of the overall conductivity under different atmospheres are shown in Fig. 9. One can observe that the lowest conductivity values are found in dry Ar in the whole temperature range studied. An enhancement of the conductivity of about one order of magnitude occurs in wet 5%H_2–Ar due to the presence of proton contribution at low temperature. As the temperature increases the material dehydrates, decreasing the protonic contribution and consequently the conductivity is less dependent on the atmosphere at high temperature. In this region, the conductivity under O_2 is higher than under 5%H_2–Ar, evidencing a significant p-type contribution. The values of conductivity (e.g. 0.014 S cm^{-1} at 700 °C in 5%H_2–Ar) are similar to those reported previously (e.g. 0.01 at 700 °C in H_2[5]).

In summary, the freeze-drying precursor method used in the present work is useful to obtain polycrystalline powder of $BaCeO_3$-based materials at temperatures as low as 800 °C. The high reactivity and sinterability of the synthesised powders allow obtaining dense ceramic materials with relative density higher than 98% at 1400 °C for 4 h. Low synthesis temperature is necessary for the synthesis of barium cerates to avoid BaO volatilization and CeO_2 segregations. Bulk and grain boundary contributions were studied under different atmospheres in the low temperature range. Grain boundary resistance depend highly on the environmental conditions at low temperature, meanwhile the bulk conductivity is less affected by the atmosphere.

Acknowledgements

This work was supported by the Spanish Research program (MAT2007-60127). The authors wish to thank Canary Islands Government for a grant of "Programa de Incorporación de doctores y tecnólogos a empresas privadas y otras entidades" (D.M.-L.) and Ministerio de Educación y Ciencia for a Ramón y Cajal fellowship (J.C.R-M). The authors are also grateful to Luis Hernández (Deparment of Inorganic Chemistry, University of La Laguna) for technical assistance.

References

1. Norby, T., Solid-state protonic conductors: principles, properties, progress and prospects. *Solid State Ionics*, 1999, **125**, 1–11.
2. Kreuer, K., Proton conductivity: materials and applications. *Chem. Mater.*, 1996, **8**, 610–641.
3. Iwahara, H., Technological challenges in the application of proton conducting ceramics, *Solid State Ionics*, 1995, **77**, 289–298.
4. Schober, T., Applications of oxidic high-temperature proton conductors. *Solid State Ionics*, 2003, **162/163**, 277–281.
5. Iwahara, H., Uchida, H., Ono, K. and Ogaki, K., Proton conduction in sintered oxides based on $BaCeO_3$. *J. Electrochem. Soc.*, 1988, **135**, 529–533.
6. Bonanos, N., Transport properties and conduction mechanism in high-temperature protonic conductors. *Solid State Ionics*, 1992, **53–56**, 967–974.
7. Iwahara, H., Asakura, Y., Katahira, K. and Tanaka, M., Prospect of hydrogen technology using proton-conducting ceramics. *Solid State Ionics*, 2004, **168**, 299–310.
8. Bonanos, N., Oxide-based protonic conductors: point defects and transport properties. *Solid State Ionics*, 2001, **145**, 265–274.
9. Kreuer, K. D., Proton-conducting oxides. *Annu. Rev. Res.*, 2003, **33**, 333–359.
10. Knight, K. S., Soar, M. and Bonanos, N., Crystal structures of gadolinium- and yttrium-doped barium cerate. *J. Mater. Chem.*, 1992, **2**, 709–712.
11. Phillips, R. J., Bonanos, N., Poulsen, F. W. and Ahlgren, E. O., Structural and electrical characterisation of $SrCe_{1-x}Y_xO_\xi$. *Solid State Ionics*, 1999, **125**, 389–395.
12. Knight, K. S., Oxygen vacancy ordering in neodymium-doped barium cerate. *Solid State Commun.*, 1999, **112**, 73–78.
13. Guan, J., Dorris, S. E., Balachandran, U. and Liu, M., The effects of dopants and A:B site nonstoichiometry on properties of Perovskite-type proton conductors. *J. Electrochem. Soc.*, 1998, **145**, 1780–1786.
14. Norby, T. and Larring, Y., Mixed hydrogen ion-electronic conductors for hydrogen permeable membranes. *Solid State Ionics*, 2000, **136–137**, 139–148.
15. Bonanos, N., Knight, K. S. and Ellis, B., Perovskite solid electrolytes: structure, transport properties and fuel cell applications. *Solid State Ionics*, 1995, **79**, 161–170.
16. Suksamai, W. and Metcalfe, I. S., Measurement of proton and oxide ion fluxes in a working Y-doped $BaCeO_3$ SOFC. *Solid State Ionics*, 2007, **178**, 627–634.
17. Lee, D. W., Won, J. H. and Shim, K. B., Low temperature synthesis of $BaCeO_3$ nano powders by the citrate process. *Mater. Lett.*, 2003, **57**, 3346–3351.
18. Agarwal, V. and Liu, M., Preparation of barium cerate-based thin films using a modified Pechini process. *J. Mater. Sci.*, 1997, **32**, 619–625.
19. Almeida de Oliveira, A. P., Hafsaoui, J., Hochepied, J.-F., Berger, M.-H. and Thorel, A., Synthesis of $BaCeO_3$ and $BaCe_{0.9}Y_{0.1}O_{3-\delta}$ from mixed oxalate precursors. *J. Eur. Ceram. Soc.*, 2007, **27**, 3597–3600.
20. Slade, R. C. T. and Singh, N., The perovskite-type proton-conducting solid electrolyte $BaCe_{0.90}Y_{0.10}O_{3-\alpha}$ in high temperature electrochemical cells. *Solid State Ionics*, 1993, **61**, 111–114.

21. Knight, K. S. and Bonanos, N., The crystal structures of some doped and undoped alkaline earth cerate perovskites. *Mater. Res. Bull.*, 1995, **30**, 347–356.
22. Ryu, K. H. and Haile, S. M., Chemical stability and proton conductivity of doped $BaCeO_3$–$BaZrO_3$ solid solutions. *Solid State Ionics*, 1999, **125**, 355–367.
23. Marrero-López, D., Peña-Martínez, J., Pérez-Coll, D. and Núñez, P., Effects of preparation method on the microstructure and transport properties of $La_2Mo_2O_9$ based materials. *J. Alloys Compd.*, 2006, **422**, 249–257.
24. El-Himri, A., Marrero-López, D. and Núñez, P., Pt_2Mo_3N and $PdPtMo_3N$: new interstitial nitrides prepared from freeze-dried precursors. *J. Solid State Chem.*, 2004, **177**, 3219–3223.
25. Iwahara, H., Yajima, T. and Ushida, H., Effect of ionic radii of dopants on mixed ionic conduction ($H^+ + O^{2-}$) in $BaCeO_3$-based electrolytes. *Solid State Ionics*, 1994, **70/71**, 267–271.
26. Liu, S., Tan, X., Li, K. and Hughes, R., Synthesis of strontium cerates-based perovskite ceramics via water-soluble complex precursor routes. *Ceram. Int.*, 2001, **28**, 327–335.
27. Rodríguez-Carvajal, J., Recent advances in magnetic structure determination by neutron powder diffraction. *Physica B: Condensed Matter.*, 1993, **192**, 55–69.
28. Roisnel, T. and Rodríguez-Carvajal, J., *WinPLOTR*. Laboratoire Léon Brillouin-LCSI, France, 2005.
29. Johnson, D., *ZView: A Software Program for IES Analysis, Version 2.8*. Scribner Associates, Inc., Southern Pines, NC, 2002.
30. Lin, H.-L., Chiang, R.-K., Kuo, C.-L. and Chang, C. W., Synthesis of $BaCeO_3$ powders by a fast aqueous citrate–nitrate process. *J. Non-Cryst. Solids*, 2007, **353**, 1188–1194.
31. Shima, D. and Haile, S. M., The influence of cation non-stoichiometry on the properties of undoped and gadolinia-doped barium cerate. *Solid State Ionics*, 1997, **97**, 443–455.
32. Hwang, S.-L. and Chem, I.-W., Grain size control of tetragonal zirconia polycrystals using the space charge concept. *J. Am. Ceram. Soc.*, 1990, **73**, 3269–3277.
33. Li, J.-G., Ikegami, T. and Mori, T., Low temperature processing of dense samrium-doped CeO_2 ceramics: sintering and grain growth behaviours. *Acta Mater.*, 2004, **52**, 2221–2228.